Green Chemical Engineering 3 (2022) 180–187

Contents lists available at ScienceDirect

Green Chemical Engineering

journal homepage: www.keaipublishing.com/en/journals/green-chemical-engineering

Article

The importance of the bite angle of metal(III) salen catalysts in the sequestration of CO_2 with epoxides in mild conditions☆

Anna Vidal-López [a,b], Sergio Posada-Pérez [a], Miquel Solà [a], Valerio D'Elia [c,*], Albert Poater [a,*]

[a] Institut de Química Computacional i Catàlisi and Departament de Química, Universitat de Girona, C/ Maria Aurèlia Capmany, 69, 17003, Girona, Catalonia, Spain
[b] Department of Chemistry, Universitat Autònoma de Barcelona, Cerdanyola del Vallès, Catalonia, 08193, Spain
[c] Department of Materials Science and Engineering, School of Molecular Science and Engineering, Vidyasirimedhi Institute of Science and Technology, (VISTEC), 21210, Payupnai, Wang Chan, Thailand

HIGHLIGHTS

- The cyclic carbonates obtained from the sustainable combination of fixing CO_2 with epoxides, by salen-based catalysts.
- Potential catalysts screened by DFT to find out the best combination between a salen ligand and a list of metal(III).
- The best catalyst, with yttrium, with a reaction pathway towards an excellent catalytic activity under mild conditions.

GRAPHICAL ABSTRACT

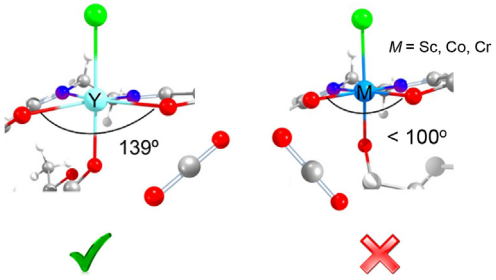

ARTICLE INFO

Keywords:
CO_2 fixation
Salen catalyst
CO_2 functionalization
Cyclic carbonate
DFT calculations
Predictive catalysis

ABSTRACT

Located in the middle of the fever to solve the problem of CO_2 emissions in the environment, CO_2 sequestration by reaction with epoxides is one of the key tools, as it not only fixes CO_2, but also makes it functional by leading to cyclic carbonates. Herein, the results are focused specifically on the formation of cyclic organic carbonates catalyzed by metal-salen complexes, previously achieved with yttrium and scandium, that are compared with those of analogous complexes containing metals from the first transition series, such as cobalt or chromium. Density functional theory (DFT) calculations allow to determine whether this switch of metals will be feasible and provide the basis for instigating future experimental efforts in this regard. The calculations analyzing the structure and electronics of the catalysts allow us to give not only a clear picture of whether these catalysts will be efficient, but also allow us to assess which metal center is the most convenient and/or whether the catalytic reaction will occur under mild conditions. Advanced buried volume calculations with the SambVca packages shed light on the different catalytic pockets of monometallic first row transition metals *vs.* group III salen complexes. Our predictive catalysis results show that the bite O-*M*-O angle plays an essential role in the catalysis.

1. Introduction

The search for environmentally sustainable and economically affordable catalysts is incessant in the world of chemistry [1,2], especially when it comes to reduce polluting gases such as CO_2. Climate change is related to the human pollution of the atmosphere due to the large volumes of anthropogenic greenhouse gases (mainly CO_2) resulting from industrial activities, transportation, etc. leading to serious

☆ Dedicated to the memory of Prof. Dr. Istvan Mayer.

* Corresponding author.
E-mail addresses: valerio.delia@vistec.ac.th (Valerio D'Elia), albert.poater@udg.edu (Albert Poater).

https://doi.org/10.1016/j.gce.2021.12.010
Received 27 October 2021; Received in revised form 14 December 2021; Accepted 27 December 2021
Available online 30 December 2021
2666-9528/© 2021 Institute of Process Engineering, Chinese Academy of Sciences. Publishing services by Elsevier B.V. on behalf of KeAi Communication Co. Ltd. This is an open access article under the CC BY-NC-ND license (http://creativecommons.org/licenses/by-nc-nd/4.0/).

environmental concerns. Among the solutions proposed to mitigate the harmful effects of CO_2, efforts from organic chemistry are based on their capture [3–6], and/or inclusion into functional molecules in order to promote their conversion towards useful chemicals [7–12]. In this context, the cycloaddition of CO_2 to epoxides to afford cyclic carbonates has experienced growing interest over the past decades [13–19]. Besides allowing the conversion of CO_2 into useful chemicals [20,21], this non-reductive process can take place under very mild conditions, *i.e.* at room temperature and relatively low CO_2 pressure ($P \leq 2$ bar) when applying the appropriate catalytic system [22–24], or by additional additives [25]. Cyclic carbonates are not only used as chemical intermediates [26–29], but they can also serve as solvents [30,31]. Whereas at the moment the demand for cyclic carbonates is not such to have a real impact on the reduction of CO_2 emission, this cycloaddition reaction represents a way to valorize CO_2 as an inexpensive feedstock [32,33].

The cycloaddition of CO_2 to epoxides requires a catalyst to overcome the significant energy barrier of epoxide ring-opening. Therefore, the process requires the presence of nucleophilic catalytic moieties generally applied in the presence of hydrogen bond donors or metal-based Lewis acids to activate the epoxide. It has recently been shown that the presence of an organocatalytic hydrogen bond donor can compete or even be more efficient than some metal catalysts [34], kinetically facilitating the reaction. Overall, a wide range of catalysts has been successfully tested, from metal complexes [35–37] to organocatalysts [38–41], including simple organic acids [42]. Organocatalysts are regarded as environmentally friendly and readily available compounds [43], but generally show lower activity than metal complexes under ambient conditions.

The variety of metalorganic complexes applied to convert epoxides into cyclic carbonates under mild conditions includes zinc porphyrins [44], calcium crown-ether complexes [45], iron bis-thioetherdiphenolates [46], sulfur-bridged bismuth bis-phenolates [47], iron(III) amine triphenolates [48], iron(II) bis-CNN pincer complexes [49], cobalt- [50], iron- [51,52], zinc/rare earths-based polymetallic complexes [53,54], aluminum heteroscorpionates [55,56], helical aluminum complexes [57], and salen-based metal complexes. Importantly, different from most ligand frameworks that require several synthetic steps, salen ligands are relatively inexpensive [58–60], as their synthesis is carried out by the facile condensation of amines/diamines [61] and salicylaldehydes followed by complexation with metal precursors [62]. Even though salen-based complexes for the cycloaddition of CO_2 to epoxides under mild conditions include metal centers such as Cr [63], Co [64], Zn [65], or Al [66–69], the obtained turnover numbers (TONs) under such conditions are generally relatively low (TON << 100).

The nature of the metal obviously has a fundamental relevance. Simple Lewis acids from group III transition metals such as YCl_3 and $ScCl_3$ are efficient catalytic components for the synthesis of cyclic carbonates [70,71]. Nevertheless, metal halides are corrosive, moisture sensitive and potentially hazardous due to the presence of several equivalents of halide per metal center [72,73]. Despite the fact that rare earth transition metals have been applied in the past in CO_2-epoxide cycloadditions with other ligands [74–76], only recently the combination of group III metals with salen ligands was explored obtaining relatively high TON values (> 140) under ambient conditions [77]. It is worth noting that in 2015, Kleij and coworkers [78] reported the copolymerization of CO_2 and cyclohexene oxide mediated by Yb(salen)-based complexes at 70 °C. Whereas previous works on salen complexes and analogous compounds involved computational studies to gain insight into the catalytic mechanism of the cycloaddition of CO_2 to epoxides [79,80], comparative studies involving rare earth metals and first-row transition metals are very rare, if existing at all, and are necessary to understand the crucial mechanistic differences between these systems.

In this work, we expand the scope of salen complexes of group III metals for the formation of cyclic carbonates from epoxides and CO_2 to first row transition metals. To keep the focus on industrially relevant substrates, epichlorohydrin and propylene oxide are chosen as epoxide reactants. Even though density functional theory (DFT) calculations here will not ensure efficient catalytic performance at atmospheric CO_2 pressure, they will provide insights towards this goal. All in all, predictive catalysis is employed in the current study, not by optimization on the ligands [81–84], or the reaction mechanism [85], but by simple substitution of the metal in monomeric salen-based catalysts [86].

2. Computational details

DFT geometry optimizations were performed at the generalized gradient approximation BP86 level [87,88], with the Gaussian09 package [89]. D3 version of Grimme (empiricaldispersion = gd3) was added to address the dispersion corrections [90]. The electronic configuration of the systems was described with the valence double-ζ with polarization (SVP) basis set for the main group atoms [91], whereas, for chromium, cobalt, scandium, yttrium, and iodine, we adopted the quasi-relativistic SDD effective core potential of Stuttgart/Dresden [92]. The reported Gibbs energies are calculated from single-point energy calculations on the BP86-D3/SVP~sdd geometries using the B3LYP functional [93], together with the D3 version of Grimme's dispersion [90] and the cc-pVTZ basis set [94]. Solvent effects were included with the Polarization Continuum Model (PCM) [95], considering propylene oxide (PO) as the solvent. The electronic energies in solvent are transformed to Gibbs energies by including the zero-point energy and thermal corrections from the gas-phase frequency calculations at the BP86/SVP~sdd level.

3. Results and discussion

With the series of monomeric metal catalysts included in Scheme 1, we performed DFT calculations at the B3LYP-D3/cc-pVTZ~sdd(pcm)//BP86/SVP~sdd computational level on the reaction pathway that leads to cyclic carbonates from sequestering CO_2 with epoxides in the presence of an iodine anion as nucleophile that is generally provided by tetra-*n*-butylammonium iodide (TBAI). The initial structure of the salen complexes was chosen based on previous experimental results with yttrium and scandium as metals and included a coordination molecule of THF. Therefore, the same initial structure was chosen for all complexes [77]. Scheme 2 includes all the intermediates and transition states involved in the reaction mechanism. There are three steps that are kinetically demanding, and in fact, in previous cases, they have been selectively the rate determining step (rds). The first is the opening of the epoxide by the nucleophilic agent [10], the second is the insertion of CO_2 [77], and the third is the closure of the cyclic carbonate [17,34,43,71]. Since there is no general trend, it is necessary to find for each catalytic system which of the three is the limiting step. In fact, simple modification of the nucleophilic agent represents a significant change in this regard [10]. The ground state for the rare earth transition metals, Sc and Y, is undoubtedly singlet, whereas for cobalt and chromium is somewhat different. For chromium, the ground state is not the doublet, but for all intermediates and transition states the quartet, being at least 13.7 and 29.7 kcal mol^{-1} above in energy the corresponding doublet and sextet homologues, respectively. For cobalt, the high spin is only present once THF is removed and before the next epoxide coordination. In detail the triplet is favoured by 1.5 and 1.8 kcal mol^{-1} for the ethyl and cyclohexyl bridge, respectively.

Starting from the octahedral environment around the M^{III} center, the THF ligand dissociates. In all cases this involves a limited destabilization that ranges from 2 to 6 kcal mol^{-1}, immediately compensated by the epoxide coordination, thus recovering the sixth ligand. Significantly, there is a higher stabilization of around 2 kcal mol^{-1} (Table 1) when dealing with propylene oxide than with epichlorohydrin, whereas the role of the bridge of the salen ligand is not relevant at all. The opening of the epoxide requires the nucleophilic attack by the iodide of TBAI. In all cases, the energy barriers do not go beyond the threshold of 20 kcal mol^{-1}. A different tendency is observed in comparison to the previous coordination

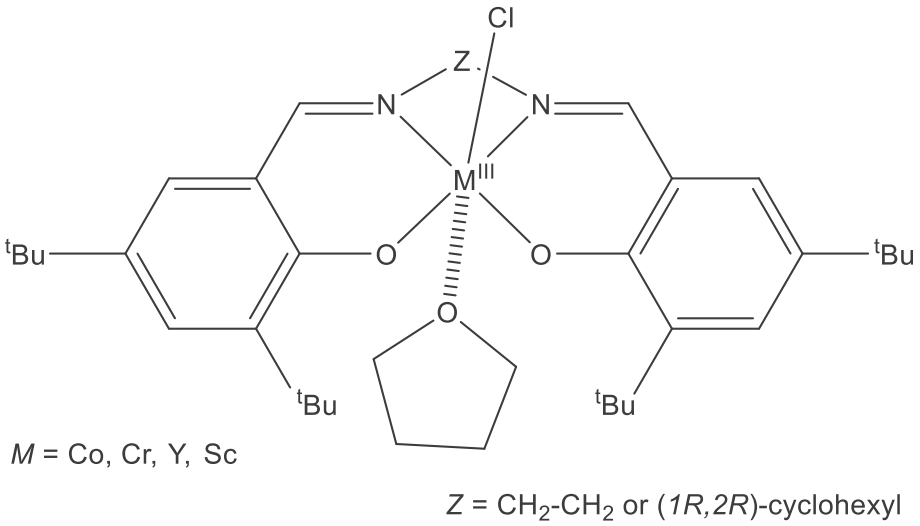

Scheme 1. Metal salen complexes are used in this study, where *M* is the metal and *Z* is the bridge.

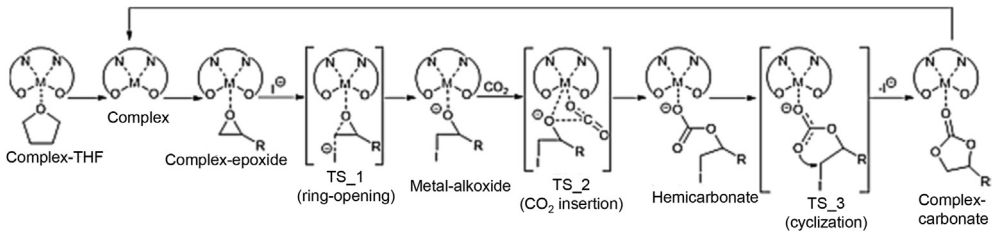

Scheme 2. Investigated mechanism of CO_2 cycloaddition to epoxides by metal salen complexes in the presence of an iodine nucleophile.

intermediate and for the transition state that leads to the metal alkoxide intermediate, since propylene oxide suffers a lower preference by 2–3 kcal mol^{-1}. This is due to the fact that epichlorohydrin bears a favorable stabilization of the closest H bond to the chloride atom of the former epoxide substrate, *i.e.* a rather strong hydrogen bond since the Cl···H distance is only around 3 Å (Fig. 1). With respect to the group III transition metals, *i.e.* yttrium and scandium, the energy barrier for the epoxide opening is 5–6 kcal mol^{-1} higher than that for chromium and cobalt, with no differences between the two epoxides analyzed. Bearing the relatively low energy barrier for this ring-opening compared to the next two steps, the nature of the countercation was not explored further, even though kinetically it was found to be important [63,66]. Next, the CO_2 insertion to generate an hemicarbonate species generally takes place with energy barriers close to 30 kcal mol^{-1}. Thus, the latter becomes the rds. However, this is not the case for yttrium (Table 1), for which the energies are close to 20 kcal mol^{-1}. Finally, the cyclic carbonate product is obtained by the closure of the previous hemicarbonate intermediate. The formed 5-membered ring shows a kinetic cost quite similar for all complexes, with respect to the initial precatalyst, ranging from 25.8 kcal mol^{-1} for the chromium complex with a cyclohexyl bridge for both substrates studied here to 29.6 kcal mol^{-1} for cobalt. This cyclization step is not more energetically demanding than the CO_2 insertion step except for cobalt with cyclohexyl bridge and epichlorohydrin as the substrate, but by only 0.2 kcal mol^{-1}. For yttrium complexes, the difference between the barriers for the CO_2 insertion and the cyclization step increases up to around 5 kcal mol^{-1}, with the CO_2 insertion step being the step with the lowest barrier.

Going into detail to explain the different performances among the series of catalysts studied in Table 1, structural and electronic features are included in Tables 2–4. First, considering the different metals under study [96,97], we calculated Mayer Bond Orders (MBOs) to better understand the evolution of the metal-oxygen bonds (M−O) in the first steps of the reaction pathway (Table 2). In particular, the coordination of the epoxide,

Table 1
Relative Gibbs energies in kcal mol^{-1}, taking the complex-THF species as the reference, for the cyclization of epoxides (epi = epichlorohydrin; prop = propylene oxide) with the metal-salen based catalysts (including the bridge: eth = C_2H_4; cyc = cyclohexyl).

	Bridge	Substrate	Complex-THF	Complex	Complex epoxide	TS_1	Metal alkoxide	TS_2	Hemicarbonate	TS_3	Complex carbonate
Co	eth	epi	0.0	4.8	1.6	11.8	6.4	30.6	13.1	29.7	2.1
Co	eth	prop	0.0	4.8	−0.4	14.3	11.2	29.3	21.1	28.4	1.3
Co	cyc	epi	0.0	5.3	1.6	11.6	6.5	29.4	13.2	29.6	2.1
Co	cyc	prop	0.0	5.3	−0.5	14.6	11.0	29.4	19.1	28.2	0.7
Cr	eth	epi	0.0	5.4	3.2	13.6	9.5	31.6	18.5	26.5	1.9
Cr	eth	prop	0.0	5.4	1.5	12.1	10.6	32.0	17.1	26.1	1.3
Cr	cyc	epi	0.0	5.9	3.0	13.4	9.6	29.2	17.7	25.8	1.5
Cr	cyc	prop	0.0	5.9	1.1	12.2	10.6	29.9	15.9	25.8	0.9
Y	eth	epi	0.0	3.5	5.1	18.8	11.6	21.0	17.5	26.2	0.3
Y	eth	prop	0.0	3.5	3.5	17.8	13.6	21.6	15.0	26.5	−0.8
Sc	eth	epi	0.0	2.2	5.2	17.3	11.7	28.1	16.7	26.6	2.0
Sc	eth	prop	0.0	2.2	2.8	19.3	13.8	29.2	15.3	27.2	−0.1
Sc	cyc	prop	0.0	2.6	2.8	19.9	14.7	30.8	16.0	27.2	−0.1

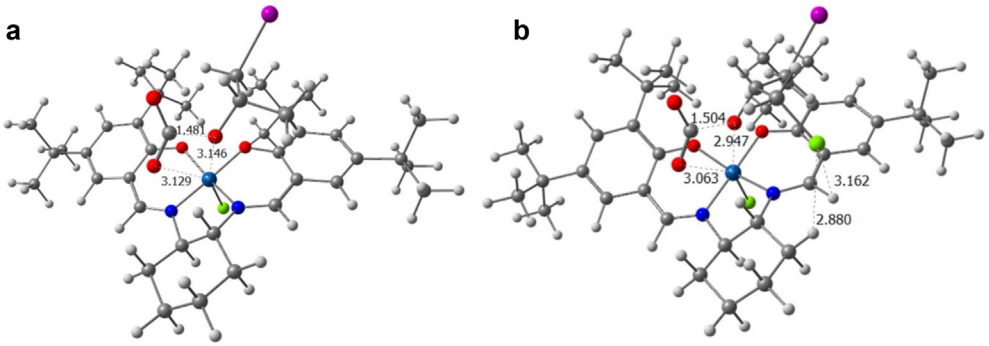

Fig. 1. Transition states TS_2, with for the complex with a cyclohexyl bridge, for Co with: (a) propylene oxide and (b) epichlorohydrin (selected distances given in Å, colours: gray (C), red (O), blue (N), white (H), green (Cl), and iodide (violet)).

ring-opening by the nucleophile and CO_2 insertion were evaluated to check the evolution of the M-$O_{epoxide}$ bond [98,99]. The stronger the M-$O_{epoxide}$ bond, especially after the opening by the iodide anion, the more difficult is the insertion of CO_2. For the metal alkoxides, it is evident that the bond between the oxygen from the epoxide and the metal is weaker for yttrium compared to the other metals, leading to easier insertion of CO_2. The MBO, but not the distances, are displayed in Table 2, given the different nature of the metal centers [3,100–102]. While the difference in the complex bearing the epoxide as a ligand is small, *i.e.* once the THF is exchanged by an epoxide reagent, being significantly lower for Y and Sc, it is an aperitif result of the biggest difference for the case of the next intermediate, *i.e.* the metal alkoxide, as it is where the smallest MBOs are seen for yttrium, and this certainly facilitates the Y–O bond to cleave more easily.

The reason for the different nature of the rds for the yttrium entries in Table 1 can be related to the fact that, structurally, the M−O and M−N bonds are much longer than for the other trivalent metals. The insertion CO_2 in the yttrium alkoxide is easier owing to the elongation of the bonds of the metal with its neighboring atoms, which causes the metal to be unable to arrange the ligands in a perfect square planar geometry to the equatorial plane, and octahedral globally. Once THF dissociates, the O–Y–O bite angle is drastically reduced from 129.2° to 108.3° although it is not related to the fact that Y regains the square planar shape (Table 3). Our simulations reveal that the metal moves away from the plane of the base of the square base pyramid. The difference in the bite angle predicted for Sc is much smaller, although significant (~15°), whereas a total lack of variation is observed for cobalt, and an insignificant variation (2-3°) for chromium. In addition, before the interaction with CO_2, the O–Y–O bite angle increases to nearly 140° in the metal alkoxide intermediate, which facilitates the pentagonal bipyramid geometry of the next TS_2. With respect to scandium, even though the O-Sc-O bite angle is again far from 90°, it is not sufficient to allocate the CO_2 molecule in the equatorial plane

Table 2
MBO for the metal-salen based catalysts.

	Bridge	Substrate	Complex epoxide						Metal alkoxide					
			M-$O_{epoxide}$	M-$N1_{salen}$	M-$N2_{salen}$	M-$O1_{salen}$	M-$O2_{salen}$	M-Cl	M-$O_{epoxide}$	M-$N1_{salen}$	M-$N2_{salen}$	M-$O1_{salen}$	M-$O2_{salen}$	M-Cl
Co	eth	epi	0.390	0.719	0.701	0.566	0.588	1.047	0.836	0.702	0.684	0.533	0.538	0.896
Co	eth	prop	0.433	0.705	0.703	0.569	0.574	1.031	0.867	0.689	0.717	0.520	0.535	0.876
Co	cyc	epi	0.394	0.733	0.704	0.568	0.592	1.063	0.836	0.710	0.684	0.534	0.545	0.921
Co	cyc	prop	0.439	0.719	0.708	0.570	0.579	1.047	0.867	0.695	0.729	0.529	0.538	0.905
Cr	eth	epi	0.332	0.564	0.560	0.488	0.517	0.889	0.755	0.541	0.517	0.453	0.491	0.753
Cr	eth	prop	0.369	0.552	0.566	0.491	0.504	0.863	0.798	0.533	0.523	0.455	0.478	0.725
Cr	cyc	epi	0.338	0.576	0.574	0.484	0.514	0.898	0.758	0.554	0.525	0.451	0.493	0.768
Cr	cyc	prop	0.377	0.560	0.581	0.486	0.500	0.871	0.804	0.560	0.581	0.486	0.500	0.737
Y	eth	epi	0.185	0.288	0.282	0.414	0.440	0.635	0.526	0.252	0.226	0.346	0.399	0.568
Y	eth	prop	0.216	0.283	0.285	0.418	0.418	0.628	0.583	0.242	0.224	0.360	0.369	0.573
Sc	eth	epi	0.254	0.477	0.503	0.634	0.647	0.838	0.639	0.433	0.443	0.534	0.583	0.764
Sc	eth	prop	0.290	0.478	0.498	0.623	0.640	0.831	0.670	0.478	0.498	0.623	0.640	0.791
Sc	cyc	prop	0.287	0.489	0.515	0.627	0.642	0.828	0.665	0.433	0.445	0.554	0.559	0.737

Table 3
O-M^{III}-O bite angle (in °) for the metal-salen based catalysts.

	Bridge	Substrate	Complex-THF	Complex	Complex epoxide	Metal alkoxide	Hemicarbonate	Complex carbonate
Co	eth	epi	85.8	85.9	86.3	87.3	85.6	85.7
Co	eth	prop	85.8	85.9	86.6	85.9	86.6	86.4
Co	cyc	epi	85.1	85.3	85.7	86.5	85.0	85.2
Co	cyc	prop	85.1	85.3	86.1	85.1	86.6	86.0
Cr	eth	epi	95.0	92.4	94.2	97.7	97.4	95.0
Cr	eth	prop	95.0	92.4	94.8	97.9	97.9	94.8
Cr	cyc	epi	93.6	91.2	93.1	96.4	96.3	93.9
Cr	cyc	prop	93.6	91.2	93.9	96.7	96.7	93.8
Y	eth	epi	129.2	108.3	122.1	139.3	135.4	129.1
Y	eth	prop	129.2	108.3	120.7	138.9	136.2	129.9
Sc	eth	epi	118.2	103.3	111.8	123.7	122.4	115.8
Sc	eth	prop	118.2	103.3	112.8	124.2	122.9	117.1
Sc	cyc	prop	115.2	100.4	111.0	126.6	119.5	112.8

Table 4
Natural population analysis on the metal and the atoms nearby for the intermediates: complex epoxide and metal alkoxide for metal-salen based catalysts. Units are electrons.

	Bridge	Substrate	Complex epoxide						Metal alkoxide					
			M	$O_{epoxide}$	$N1_{salen}$	$N2_{salen}$	$O1_{salen}$	$O2_{salen}$	Cl	M	$O_{epoxide}$	$N1_{salen}$	$N2_{salen}$	$O1_{salen}$	$O2_{salen}$	Cl
Co	eth	epi	0.540	−0.459	−0.382	−0.385	−0.630	−0.606	−0.376	0.539	−0.671	−0.358	−0.358	−0.613	−0.605	−0.521
Co	eth	prop	0.534	−0.464	−0.375	−0.380	−0.627	−0.606	−0.391	0.544	−0.674	−0.366	−0.356	−0.590	−0.601	−0.526
Co	cyc	epi	0.561	−0.460	−0.385	−0.388	−0.634	−0.609	−0.380	0.560	−0.673	−0.360	−0.361	−0.617	−0.609	−0.523
Co	cyc	prop	0.556	−0.465	−0.377	−0.383	−0.631	−0.609	−0.395	0.564	−0.677	−0.371	−0.359	−0.591	−0.602	−0.528
Cr	eth	epi	0.792	−0.478	−0.476	−0.476	−0.681	−0.662	−0.364	0.828	−0.741	−0.456	−0.452	−0.673	−0.661	−0.479
Cr	eth	prop	0.787	−0.491	−0.466	−0.472	−0.676	−0.661	−0.369	0.824	−0.742	−0.450	−0.449	−0.668	−0.661	−0.489
Cr	cyc	epi	0.817	−0.478	−0.481	−0.482	−0.685	−0.666	−0.365	0.855	−0.743	−0.463	−0.459	−0.677	−0.665	−0.481
Cr	cyc	prop	0.814	−0.491	−0.472	−0.479	−0.681	−0.665	−0.370	0.852	−0.744	−0.457	−0.456	−0.671	−0.665	−0.491
Y	eth	epi	1.766	−0.524	−0.585	−0.579	−0.840	−0.838	−0.587	1.696	−0.885	−0.569	−0.562	−0.795	−0.803	−0.636
Y	eth	prop	1.762	−0.546	−0.576	−0.578	−0.838	−0.832	−0.587	1.704	−0.895	−0.560	−0.560	−0.799	−0.798	−0.641
Sc	eth	epi	1.284	−0.503	−0.523	−0.528	−0.773	−0.765	−0.464	1.251	−0.805	−0.511	−0.504	−0.743	−0.750	−0.561
Sc	eth	prop	1.275	−0.519	−0.521	−0.525	−0.770	−0.762	−0.468	1.246	−0.804	−0.501	−0.503	−0.738	−0.741	−0.574
Sc	cyc	prop	1.307	−0.518	−0.526	−0.531	−0.775	−0.768	−0.475	1.261	−0.814	−0.508	−0.516	−0.742	−0.746	−0.561

(Fig. 2). The TS_2 for rare earth transition metals have a different nature than for the first row transition metals. For the latter, CO_2 enjoys lower steric repulsion and favorable H-bonds above any of the M−O bonds while for Y and Sc the greater O-*M*-O bite angle allows, in both cases, the approach of CO_2 through that cleft that fits in the O-*M*-O angle. In addition, this observation is in agreement with the dimeric structures only found for such group III transition metals [77]. Knowing that the atomic radius of yttrium is 180 Å and of scandium 162 Å, whereas it is only 125 and 128 Å for cobalt and chromium, respectively, it is clear that the O-*M*-O angle is completely related to the size of the metal ion, but this is true thanks to the chelated tetradentate ligand used here. On the other hand, alternative transition states were computed, with partial dissociation or cleavage of any of the M−O or M−N bonds, being all higher in energy by at least 10 kcal mol^{-1}. Thus, it is mandatory that the metal keeps stable its equatorial plane. In addition, the SambVca steric maps, developed by Cavallo and collaborators [103,104], were made in the plane perpendicular to that which includes the metal and the 4 coordinating atoms of the ligand, using propylene oxide as a substrate (Table S1). This plane is placed 2.0 Å away from the metal, as it is the area of space where CO_2 inserts. Resulting from the steric maps, the V_{Bur}% was also calculated, being the amount of the first coordination sphere of the metal occupied by a given ligand [105,106]. For cobalt, the calculated V_{Bur}% for the initial complex, *i.e.* the complex obtained after THF exchange by epoxide, is 92.2%, which confirms that there is no possibility for CO_2 insertion since the angle O–Co–O is too closed to fit CO_2, *i.e.* in the space left by the two oxygen atoms. Same conclusion is reached for chromium with a V_{Bur}% value of 89.5%. A significant reduction is obtained for the Sc complex (73.4%) and much more for the Y complex, with a value of 66.9%. Even though the steric maps are not sufficiently clear (Table S1), the difference in V_{Bur}% is significant, which confirms that the bite angle O-*M*-O for yttrium is the most accentuated.

The results in Table 4 regarding Natural Bond Orbital (NBO) charges reinforce the idea that rare earth metals are much more positively charged at their metallic center, especially in the case of yttrium. In fact, the charge varies on average within a range starting at 0.5 for Co, going from 0.8 for Cr, 1.3 for Sc, to 1.8 for Y. However, it should also be emphasized that the oxygen charge of any of both epoxides is almost invariable, within less than 0.1 e, and ranges from −0.46 for Co to a maximum of −0.55 for Y. The same would be true for the chlorine atom located *trans* to the epoxide. For the other atoms of the tetradentate ligand, there is a noticeable difference, up to 0.2 e from Co and Cr to Sc and with Y showing the most negative values. Although the higher negative charge on the metal due to the oxygen in the salen ligand cannot compensate for the charge of the metal, yttrium will have the highest tendency at the electronic level to insert CO_2.

Going to the frontier molecular orbitals theory, there is no significant difference between the values of Co, Sc, and Y, paying attention only to singlet complexes, for not having to make use of the theory of SOMO orbitals, for Co and Cr, with its associated complexity [107].

4. Conclusions

Based on solid results at the experimental level regarding the catalytic role of salen monometallic complexes of scandium and yttrium as Lewis acids for the cycloaddition of CO_2 to epoxides, a comparative theoretical study has been carried out involving transition metals of the first-row that were also previously employed in salen complexes for the same reaction. The results of the kinetics of all compounds indicate that the reaction would require moderate temperature, and the path towards room temperature is open, in agreement with past experiments based on rare earth metals [77]. This predictive catalysis effort has been made on industrially attractive epoxides such as epichlorohydrin and propylene oxide. Our simulations reveal different rate limiting step for the CO_2 cycloaddition as a function of the metal used in the salen complexes. For Co, Cr, and Sc, the CO_2 insertion becomes the most energy demanding step, whereas Y facilitates the CO_2 adduct formation thanks to the greater

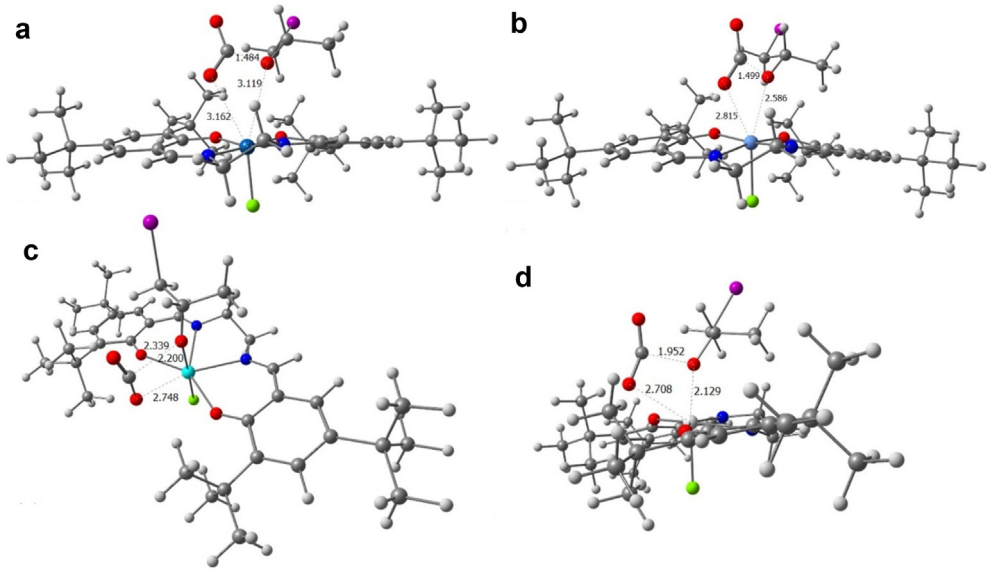

Fig. 2. Transition states TS_2, with ethyl as a bridge, for propylene oxide for (a) Co, (b) Cr, (c) Sc and (d) Y (selected distances given in Å, colours: gray (C), red (O), blue (N), white (H), green (Cl), and iodide (violet)).

bite angle. The mechanistic investigations show that the closure of the carbonate ring is the rate determining step when using Y. To sum up, this study explains the improved catalytic activity of early transition metals compared to first-row transition metals, and it has been possible to find out why yttrium is the candidate that requires less kinetic effort. Overall, in the context of CO_2 fixation, this work suggests that metal centers with large atomic radius may facilitate the step of CO_2 insertion due to the greater bite angle that it entails.

Declaration of competing interests

The authors declare that they have no known competing financial interests or personal relationships that could have appeared to influence the work reported in this paper.

Acknowledgements

S.P.P. thanks the Spanish Ministerio de Ciencia e Innovacion for Juan de la Cierva Formación fellowship (FJC2019-039623-I). A.P. is a Serra Húnter Fellow and ICREA Academia Prize 2019. M.S. and A.P. thank the Spanish MINECO for projects PID2020-113711GB-I00, PID2021-127423NB-I00, and PGC2018-097722-B-I00 and the Generalitat de Catalunya for project 2017SGR39.

Appendix A. Supplementary data

Supplementary data to this article can be found online at https://doi.org/10.1016/j.gce.2021.12.010.

References

[1] C. Mora, D. Spirandelli, E.C. Franklin, J. Lynham, M.B. Kantar, W. Miles, C.Z. Smith, K. Freel, J. Moy, L.V. Louis, E.W. Barba, K. Bettinger, A.G. Frazier, J.F. Colburn IX, N. Hanasaki, E. Hawkins, Y. Hirabayashi, W. Knorr, C.M. Little, K. Emanuel, J. Sheffield, J.A. Patz, C.L. Hunter, Broad threat to humanity from cumulative climate hazards intensified by greenhouse gas emissions, Nat. Clim. Change 8 (2018) 1062–1071.

[2] J.S. Gregg, R.J. Andres, G. Marland, China: emissions pattern of the world leader in CO_2 emissions from fossil fuel consumption and cement production, Geophys. Res. Lett. 35 (2008) L08806.

[3] J. Poater, M. Gimferrer, A. Poater, Covalent and ionic capacity of MOFs to sorb small gas molecules, Inorg. Chem. 57 (2018) 6981–6990.

[4] A.R. Shaikh, M. Ashraf, T. AlMayef, M. Chawla, A. Poater, L. Cavallo, Amino acid ionic liquids as potential candidates for CO_2 capture: combined density functional theory and molecular dynamics simulations, Chem. Phys. Lett. 745 (2020) 137239.

[5] N. Mac Dowell, P.S. Fennell, N. Shah, G.C. Maitland, The role of CO_2 capture and utilization in mitigating climate change, Nat. Clim. Change 7 (2017) 243–249.

[6] M. Fallah, N. Bahri-Laleh, K. Didehban, A. Poater, Interaction of common cocatalysts in Ziegler-Natta catalyzed olefin polymerization, Appl. Organomet. Chem. 34 (2020) e5333.

[7] L. Song, Y.-X. Jiang, Z. Zhang, Y.-Y. Gui, X.-Y. Zhou, D.-G. Yu, $CO_2 = CO + [O]$: recent advances in carbonylation of C–H bonds with CO_2, Chem. Commun. 56 (2020) 8355–8367.

[8] C.-K. Ran, X.-W. Chen, Y.-Y. Gui, J. Liu, L. Song, K. Ren, D.-G. Yu, Recent advances in asymmetric synthesis with CO_2, Sci. China Chem. 63 (2020) 1336–1351.

[9] N.A. Tappe, R.M. Reich, V. D'Elia, F.E. Kühn, Current advances in the catalytic conversion of carbon dioxide by molecular catalysts: an update, Dalton Trans. 47 (2018) 13281–13313.

[10] W. Natongchai, J.A. Luque-Urrutia, C. Phungpanyia, M. Solà, V. D'Elia, A. Poater, H. Zipse, Cycloaddition of CO_2 to epoxides by highly nucleophilic 4-aminopyridines: establishing a relationship between carbon basicity and catalytic performance by experimental and DFT investigations, Org. Chem. Front. 8 (2021) 613–627.

[11] S. Arayachukiat, P. Yingcharoen, S.V.C. Vummaleti, L. Cavallo, A. Poater, V. D'Elia, Cycloaddition of CO_2 to challenging N-tosyl aziridines using a halogen-free niobium complex: catalytic activity and mechanistic insights, Mol. Catal. 443 (2017) 280–285.

[12] S. Coufourier, Q. Gaignard-Gaillard, J.-F. Lohier, A. Poater, S. Gaillard, J.-L. Renaud, Hydrogenation of CO_2, hydrogenocarbonate, and carbonate to formate in water using phosphine free bifunctional iron complexes, ACS Catal. 10 (2020) 2108–2116.

[13] C. Martín, G. Fiorani, A.W. Kleij, Recent advances in the catalytic preparation of cyclic organic carbonates, ACS Catal. 5 (2015) 1353–1370.

[14] V. D'Elia, J.D.A. Pelletier, J.-M. Basset, Cycloadditions to epoxides catalyzed by group III-V transition-metal complexes, ChemCatChem 7 (2015) 1906–1917.

[15] J.W. Comerford, I.D.V. Ingram, M. North, X. Wu, Sustainable metal-based catalysts for the synthesis of cyclic carbonates containing five-membered rings, Green Chem. 17 (2015) 1966–1987.

[16] F. Della Monica, A. Buonerba, C. Capacchione, Homogeneous iron catalysts in the reaction of epoxides with carbon dioxide, Adv. Synth. Catal. 361 (2019) 265–282.

[17] V. D'Elia, A.A. Ghani, A. Monassier, J. Sofack-Kreutzer, J.D.A. Pelletier, M. Drees, S.V.C. Vummaleti, A. Poater, L. Cavallo, M. Cokoja, J.-M. Basset, F.E. Kühn, Dynamics of the $NbCl_5$-catalyzed cycloaddition of propylene oxide and CO_2: assessing the dual role of the nucleophilic co-catalysts, Chem. Eur. J. 20 (2014) 11870–11882.

[18] V. Aomchad, À. Cristòfol, F. Della Monica, B. Limburg, V. D'Elia, A.W. Kleij, Recent progress in the catalytic transformation of carbon dioxide into biosourced organic carbonates, Green Chem. 23 (2021) 1077–1113.

[19] W. Al Maksoud, A. Saidi, M.K. Samantaray, E. Abou-Hamad, A. Poater, S. Ould-Chikh, X. Guo, E. Guan, T. Ma, B.C. Gates, J.-M. Basset, Docking of tetra-methyl zirconium to the surface of silica: a well-defined pre-catalyst for conversion of CO_2 to cyclic carbonate, Chem. Commun. 56 (2020) 3528–3531.

[20] J. Artz, T.E. Müller, K. Thenert, J. Kleinekorte, R. Meys, A. Sternberg, A. Bardow, W. Leitner, Sustainable conversion of carbon dioxide: an integrated review of catalysis and life cycle assessment, Chem. Rev. 118 (2017) 434–504.

[21] Q.-W. Song, Z.-H. Zhou, L.-N. He, Efficient, selective and sustainable catalysis of carbon dioxide, Green Chem. 19 (2017) 3707–3728.

[22] M.J. Kelly, A. Barthel, C. Maheu, O. Sodpiban, F.-B. Dega, S.V.C. Vummaleti, E. Abou-Hamad, J.D.A. Pelletier, L. Cavallo, V. D'Elia, J.-M. Basset, Conversion of actual flue gas CO_2 *via* cycloaddition to propylene oxide catalyzed by a singlesite, recyclable zirconium catalyst, J. CO_2 Util. 20 (2017) 243–252.

[23] H. Büttner, L. Longwitz, J. Steinbauer, C. Wulf, T. Werner, Recent developments in the synthesis of cyclic carbonates from epoxides and CO_2, Top. Curr. Chem. 375 (2017) 50.

[24] R.R. Shaikh, S. Pornpraprom, V. D'Elia, Catalytic strategies for the cycloaddition of pure, diluted, and waste CO_2 to epoxides under ambient conditions, ACS Catal. 8 (2018) 419–450.

[25] W. Zhang, F. Ma, L. Ma, Y. Zhou, J. Wang, Imidazolium-functionalized ionic hypercrosslinked porous polymers for efficient synthesis of cyclic carbonates from simulated flue gas, ChemSusChem 13 (2020) 341–350.

[26] S. Fukuoka, M. Kawamura, K. Komiya, M. Tojo, H. Hachiya, K. Hasegawa, M. Aminaka, H. Okamoto, I. Fukawa, S. Konno, A novel non-phosgene polycarbonate production process using by-product CO_2 as starting material, Green Chem. 5 (2003) 497–507.

[27] N. Yadav, F. Seidi, D. Crespy, V. D'Elia, Polymers based on cyclic carbonates as trait d'Union between polymer chemistry and sustainable CO_2 utilization, ChemSusChem 12 (2019) 724–754.

[28] W. Guo, J.E. Gómez, À. Cristòfol, J. Xie, A.W. Kleij, Catalytic transformations of functionalized cyclic organic carbonates, Angew. Chem. Int. Ed. 57 (2018) 13735–13747.

[29] A.J. Kamphuis, F. Picchioni, P.P. Pescarmona, CO_2-fixation into cyclic and polymeric carbonates: principles and applications, Green Chem. 21 (2019) 406–448.

[30] B. Schäffner, F. Schäffner, S.P. Verevkin, A. Börner, Organic carbonates as solvents in synthesis and catalysis, Chem. Rev. 110 (2010) 4554–4581.

[31] S.B. Lawrenson, R. Arav, M. North, The greening of peptide synthesis, Green Chem. 19 (2017) 1685–1691.

[32] J. Li, D. Jia, Z. Guo, Y. Liu, Y. Lyu, Y. Zhou, J. Wang, Imidazolinium based porous hypercrosslinked ionic polymers for efficient CO_2 capture and fixation with epoxides, Green Chem. 19 (2017) 2675–2686.

[33] Z. Guo, Q. Jiang, Y. Shi, J. Li, X. Yang, W. Hou, Y. Zhou, J. Wang, Tethering dual hydroxyls into mesoporous poly(ionic liquid)s for chemical fixation of CO_2 at ambient conditions: a combined experimental and theoretical study, ACS Catal. 7 (2017) 6770–6780.

[34] S. Arayachukiat, C. Kongtes, A. Barthel, S.V.C. Vummaleti, A. Poater, S. Wannakao, L. Cavallo, V. D'Elia, Ascorbic acid as a bifunctional hydrogen bond donor for the synthesis of cyclic carbonates from CO_2 under ambient conditions, ACS Sustain. Chem. Eng. 5 (2017) 6392–6397.

[35] H. Kisch, R. Millini, I.-J. Wang, Bifunktionelle katalysatoren zur synthese cyclischer carbonate aus oxiranen und kohlendioxid, Chem. Ber. 119 (1986) 1090–1094.

[36] B. Dutta, J. Sofack-Kreutzer, A.A. Ghani, V. D'Elia, J.D.A. Pelletier, M. Cokoja, F.E. Kühn, J.-M. Basset, Nucleophile-directed selectivity towards linear carbonates in the niobium pentaethoxide-catalysed cycloaddition of CO_2 and propylene oxide, Catal. Sci. Technol. 4 (2014) 1534–1538.

[37] K.A. Andrea, F.M. Kerton, Triaryl borane catalyzed formation of cyclic organic carbonates and polycarbonates, ACS Catal. 9 (2019) 1799–1809.

[38] M. Cokoja, M.E. Wilhelm, M.H. Anthofer, W.A. Herrmann, F.E. Kühn, Synthesis of cyclic carbonates from epoxides and carbon dioxide by using organocatalysts, ChemSusChem 8 (2015) 2436–2454.

[39] S. Sopeña, E. Martin, E.C. Escudero-Adán, A.W. Kleij, Pushing the limits with squaramide-based organocatalysts in cyclic carbonate synthesis, ACS Catal. 7 (2017) 3532–3539.

[40] C. Maeda, K. Ogawa, K. Sadanaga, K. Takaishi, T. Ema, Chiroptical and catalytic properties of doubly binaphthyl-strapped chiral porphyrins, Chem. Commun. 55 (2019) 1064–1067.

[41] N. Liu, Y.-F. Xie, C. Wang, S.-J. Li, D. Wei, M. Li, B. Dai, Cooperative multifunctional organocatalysts for ambient conversion of carbon dioxide into cyclic carbonates, ACS Catal. 8 (2018) 9945–9957.

[42] M. Alves, B. Grignard, R. Mereau, C. Jerome, T. Tassaing, C. Detrembleur, Organocatalyzed coupling of carbon dioxide with epoxides for the synthesis of cyclic carbonates: catalyst design and mechanistic studies, Catal. Sci. Technol. 7 (2017) 2651–2684.

[43] P. Yingcharoen, C. Kongtes, S. Arayachukiat, K. Suvarnapunya, S.V.C. Vummaleti, S. Wannakao, L. Cavallo, A. Poater, V. D'Elia, Assessing the pK_a-dependent activity of hydroxyl hydrogen bond donors in the organocatalyzed cycloaddition of carbon dioxide to epoxides: experimental and theoretical study, Adv. Synth. Catal. 361 (2019) 366–373.

[44] C. Maeda, J. Shimonishi, R. Miyazaki, J. Hasegawa, T. Ema, Highly active and robust metalloporphyrin catalysts for the synthesis of cyclic carbonates from a broad range of epoxides and carbon dioxide, Chem. Eur. J. 22 (2016) 6556–6563.

[45] J. Steinbauer, A. Spannenberg, T. Werner, An *in situ* formed Ca^{2+}–crown ether complex and its use in CO_2-fixation reactions with terminal and internal epoxides, Green Chem. 19 (2017) 3769–3779.

[46] F. Della Monica, B. Maity, T. Pehl, A. Buonerba, A. De Nisi, M. Monari, A. Grassi, B. Rieger, L. Cavallo, C. Capacchione, [OSSO]-type iron(III) complexes for the low-pressure reaction of carbon dioxide with epoxides: catalytic activity, reaction kinetics, and computational study, ACS Catal. 8 (2018) 6882–6893.

[47] S.-F. Yin, S. Shimada, Synthesis and structure of bismuth compounds bearing a sulfur-bridged bis(phenolato) ligand and their catalytic application to the solvent free synthesis of propylene carbonate from CO_2 and propylene oxide, Chem. Commun. (2009) 1136–1138.

[48] C.J. Whiteoak, E. Martin, M.M. Belmonte, J. Benet-Buchholz, A.W. Kleij, An efficient iron catalyst for the synthesis of five- and six-membered organic carbonates under mild conditions, Adv. Synth. Catal. 354 (2012) 469–476.

[49] F. Chen, N. Liu, B. Dai, Iron(II) bis-CNN pincer complex-catalyzed cyclic carbonate synthesis at room temperature, ACS Sustainable Chem. Eng. 5 (2017) 9065–9075.

[50] D. De, A. Bhattacharyya, P.K. Bharadwaj, Enantioselective aldol reactions in water by a proline-derived cryptand and fixation of CO_2 by its exocyclic Co(II) complex, Inorg. Chem. 56 (2017) 11443–11449.

[51] C.K. Karan, M. Bhattacharjee, Two iron complexes as homogeneous and heterogeneous catalysts for the chemical fixation of carbon dioxide, Inorg. Chem. 57 (2018) 4649–4656.

[52] A. Buchard, M.R. Kember, K.G. Sandeman, C.K. Williams, A bimetallic iron(III) catalyst for CO_2/epoxide coupling, Chem. Commun. 47 (2011) 212–214.

[53] L. Wang, C. Xu, Q. Han, X. Tang, P. Zhou, R. Zhang, G. Gao, B. Xu, W. Qin, W. Liu, Ambient chemical fixation of CO_2 using a highly efficient heterometallic helicate catalyst system, Chem. Commun. 54 (2018) 2212–2215.

[54] G. Gao, L. Wang, R. Zhang, C. Xu, H. Yang, W. Liu, Hexanuclear 3d–4f complexes as efficient catalysts for converting CO_2 into cyclic carbonates, Dalton Trans. 48 (2019) 3941–3945.

[55] J. Martínez, J.A. Castro-Osma, A. Earlam, C. Alonso-Moreno, A. Otero, A. Lara-Sánchez, M. North, A. Rodríguez-Diéguez, Synthesis of cyclic carbonates catalysed by aluminium heteroscorpionate complexes, Chem. Eur. J. 21 (2015) 9850–9862.

[56] J. Martínez, F. de la Cruz-Martínez, M.A. Gaona, E. Pinilla-Peñalver, J. Fernández-Baeza, A.M. Rodríguez, J.A. Castro-Osma, A. Otero, A. Lara-Sánchez, Influence of the counterion on the synthesis of cyclic carbonates catalyzed by bifunctional aluminum complexes, Inorg. Chem. 58 (2019) 3396–3408.

[57] M.A. Gaona, F. de la Cruz-Martínez, J. Fernández-Baeza, L.F. Sánchez-Barba, C. Alonso-Moreno, A.M. Rodríguez, A. Rodríguez-Diéguez, J.A. Castro-Osma, A. Otero, A. Lara-Sánchez, Synthesis of helical aluminium catalysts for cyclic carbonate formation, Dalton Trans. 48 (2019) 4218–4227.

[58] A. Decortes, A.M. Castilla, A.W. Kleij, Salen-complex-mediated formation of cyclic carbonates by cycloaddition of CO_2 to epoxides, Angew. Chem. Int. Ed. 49 (2010) 9822–9837.

[59] A. Coletti, C.J. Whiteoak, V. Conte, A.W. Kleij, Vanadium catalyzed synthesis of cyclic organic carbonates, ChemCatChem 4 (2012) 1190–1196.

[60] A. Kilic, M. Durgun, M. Ulusoy, E. Tas, Conversion of CO_2 into cyclic carbonates in the presence of metal complexes as catalysts, J. Chem. Res. 34 (2010) 622–626.

[61] A. Kilic, E. Yasar, E. Aytar, Neutral boron $[(L_{1\text{-}3})BPh_2]$ and cationic charged boron $[(L_{1a\text{-}3a})BPh_2]$ complexes for chemical CO_2 conversion to obtain cyclic carbonates under ambient conditions, Sustain. Energy Fuels 3 (2019) 1066–1077.

[62] T.P. Yoon, Privileged chiral catalysts, Science 299 (2003) 1691–1693.

[63] J.A. Castro-Osma, K.J. Lamb, M. North, Cr(salophen) complex catalyzed cyclic carbonate synthesis at ambient temperature and pressure, ACS Catal. 6 (2016) 5012–5025.

[64] F. Zhou, S.-L. Xie, X.-T. Gao, R. Zhang, C.-H. Wang, G.-Q. Yin, J. Zhou, Activation of (salen)Co^{I} complex by phosphorane for carbon dioxide transformation at ambient temperature and pressure, Green Chem. 19 (2017) 3908–3915.

[65] M. Taherimehr, A. Decortes, S.M. Al-Amsyar, W. Lueangchaichaweng, C.J. Whiteoak, E.C. Escudero-Adán, A.W. Kleij, P.P. Pescarmona, A highly active Zn(salphen) catalyst for production of organic carbonates in a green CO_2 medium, Catal. Sci. Technol. 2 (2012) 2231–2237.

[66] J. Meléndez, M. North, P. Villuendas, One-component catalysts for cyclic carbonate synthesis, Chem. Commun. (2009) 2577–2579.

[67] W. Clegg, R.W. Harrington, M. North, R. Pasquale, Cyclic carbonate synthesis catalysed by bimetallic aluminium-salen complexes, Chem. Eur. J. 16 (2010) 6828–6843.

[68] J.A. Castro-Osma, M. North, X. Wu, Synthesis of cyclic carbonates catalysed by chromium and aluminium salphen complexes, Chem. Eur. J. 22 (2016) 2100–2107.

[69] J. Meléndez, M. North, R. Pasquale, Synthesis of cyclic carbonates from atmospheric pressure carbon dioxide using exceptionally active aluminium(salen) complexes as catalysts, Eur. J. Inorg. Chem. 2007 (2007) 3323–3326.

[70] A. Barthel, Y. Saih, M. Gimenez, J.D.A. Pelletier, F.E. Kühn, V. D'Elia, J.-M. Basset, Highly integrated CO_2 capture and conversion: direct synthesis of cyclic carbonates from industrial flue gas, Green Chem. 18 (2016) 3116–3123.

[71] O. Sodpiban, S. Del Gobbo, S. Barman, V. Aomchad, P. Kidkhunthod, S. Ould-Chikh, A. Poater, V. D'Elia, J.-M. Basset, Synthesis of well-defined yttrium-based Lewis acids by capture of a reaction intermediate and catalytic application for cycloaddition of CO_2 to epoxides under atmospheric pressure, Catal. Sci. Technol. 9 (2019) 6152–6165.

[72] I.D.V. Ingram, M. North, X. Wu, Halide-free synthesis of cyclic and polycarbonates, in: P. Tundo, L.-N. He, E. Lokteva, C. Mota (Eds.), Chemistry beyond Chloride, Springer International Publishing, Switzerland, 2016, pp. 413–434.

[73] A.W. Kleij, Advancing halide-free catalytic synthesis of CO_2 based heterocycles, Curr. Opin. Green Sustain. Chem. 24 (2020) 72–81.

[74] B. Xu, P. Wang, M. Lv, D. Yuan, Y. Yao, Transformation of carbon dioxide into oxazolidinones and cyclic carbonates catalyzed by rare-earth-metal phenolates, ChemCatChem 8 (2016) 2466–2471.

[75] J. Qin, P. Wang, Q. Li, Y. Zhang, D. Yuan, Y. Yao, Catalytic production of cyclic carbonates mediated by lanthanide phenolates under mild conditions, Chem. Commun. 50 (2014) 10952–10955.

[76] L. Qu, I. del Rosal, Q. Li, Y. Wang, D. Yuan, Y. Yao, L. Maron, Efficient CO_2 transformation under ambient condition by heterobimetallic rare earth complexes: experimental and computational evidences of asynergistic effect, J. CO_2 Util. 33 (2019) 413–418.

[77] V. Aomchad, S. Del Globo, A. Poater, V. D'Elia, Exploring the potential of Group III salen complexes for the conversion of CO_2 under ambient conditions, Catal. Today 375 (2021) 324–334.
[78] A. Decortes, R.M. Haak, C. Martín, M.M. Belmonte, E. Martin, J. Benet-Buchholz, A.W. Kleij, Copolymerization of CO_2 and cyclohexene oxide mediated by Yb(salen)-based complexes, Macromolecules 48 (2015) 8197–8207.
[79] F. Castro-Gómez, G. Salassa, A.W. Kleij, C. Bo, A DFT study on the mechanism of the cycloaddition reaction of CO_2 to epoxides catalyzed by Zn(salphen) complexes, Chem. Eur. J. 19 (2013) 6289–6298.
[80] T.-T. Wang, Y. Xie, W.-Q. Deng, Reaction mechanism of epoxide cycloaddition to CO_2 catalyzed by salen-*M* (*M* = Co, Al, Zn), J. Phys. Chem. 118 (2014) 9239–9243.
[81] M. Tomasini, J. Duran, S. Simon, L.M. Azofra, A. Poater, Towards mild conditions by predictive catalysis *via* sterics in the Ru-catalyzed hydrogenation of thioesters, Mol. Catal. 510 (2021) 111692.
[82] S. Escayola, J. Poater, M. Ramos, J.A. Luque-Urrutia, J. Duran, S. Simon, M. Solà, L. Cavallo, S.P. Nolan, A. Poater, Chelation enforcing a dual gold configuration in the catalytic hydroxyphenoxylation of alkynes, Appl. Organomet. Chem. (2021) e6362.
[83] S. Escayola, M. Solà, A. Poater, Mechanism of the facile nitrous oxide fixation by homogeneous ruthenium hydride pincer catalysts, Inorg. Chem. 59 (2020) 9374–9383.
[84] J.A. Luque-Urrutia, A. Poater, The fundamental non innocent role of water for the hydrogenation of nitrous oxide by PNP pincer Ru-based catalysts, Inorg. Chem. 56 (2017) 14383–14387.
[85] A. Gómez-Suárez, Y. Oonishi, A.R. Martin, S.V.C. Vummaleti, D.J. Nelson, D.B. Cordes, A.M.Z. Slawin, L. Cavallo, S.P. Nolan, A. Poater, On the mechanism of the digold(I)-hydroxide-catalysed hydrophenoxylation of alkynes, Chem. Eur. J. 22 (2016) 1125–1132.
[86] A. Poater, S.V.C. Vummaleti, E. Pump, L. Cavallo, Comparing Ru and Fe-catalyzed olefin metathesis, Dalton Trans. 43 (2014) 11216–11220.
[87] A.D. Becke, Density-functional exchange-energy approximation with correct asymptotic behavior, Phys. Rev. 38 (1988) 3098–3100.
[88] J.P. Perdew, Density-functional approximation for the correlation energy of the inhomogeneous electron gas, Phys. Rev. B 33 (1986) 8822–8824.
[89] M.J. Frisch, G.W. Trucks, H.B. Schlegel, G.E. Scuseria, M.A. Robb, J.R. Cheeseman, G. Scalmani, V. Barone, G.A. Petersson, H. Nakatsuji, X. Li, M. Caricato, A. Marenich, J. Bloino, B.G. Janesko, R. Gomperts, B. Mennucci, H.P. Hratchian, J.V. Ortiz, A.F. Izmaylov, J.L. Sonnenberg, D. Williams-Young, F. Ding, F. Lipparini, F. Egidi, J. Goings, B. Peng, A. Petrone, T. Henderson, D. Ranasinghe, V.G. Zakrzewski, J. Gao, N. Rega, G. Zheng, W. Liang, M. Hada, M. Ehara, K. Toyota, R. Fukuda, J. Hasegawa, M. Ishida, T. Nakajima, Y. Honda, O. Kitao, H. Nakai, T. Vreven, K. Throssell, J.A. Montgomery Jr., J.E. Peralta, F. Ogliaro, M. Bearpark, J.J. Heyd, E. Brothers, K.N. Kudin, V.N. Staroverov, T. Keith, R. Kobayashi, J. Normand, K. Raghavachari, A. Rendell, J.C. Burant, S.S. Iyengar, J. Tomasi, M. Cossi, J.M. Millam, M. Klene, C. Adamo, R. Cammi, J.W. Ochterski, R.L. Martin, K. Morokuma, O. Farkas, J.B. Foresman, D.J. Fox, Gaussian 09 Revision D.01, Gaussian, Inc., 2016. Wallingford CT.
[90] S. Grimme, J. Antony, S. Ehrlich, H. Krieg, A consistent and accurate ab initio parametrization of density functional dispersion correction (DFT-D) for the 94 elements H-Pu, J. Chem. Phys. 132 (2010) 154104.
[91] A. Schäfer, H. Horn, R. Ahlrichs, Fully optimized contracted Gaussian basis sets for atoms Li to Kr, J. Chem. Phys. 97 (1992) 2571–2577.
[92] A. Bergner, M. Dolg, W. Küchle, H. Stoll, H. Preuß, Ab initio energy-adjusted pseudopotentials for elements of groups 13–17, Mol. Phys. 80 (2006) 1431–1441.
[93] A.D. Becke, Density-functional thermochemistry. III. The role of exact exchange, J. Chem. Phys. 98 (1993) 5648–5652.
[94] R.A. Kendall, T.H. Dunning, R.J. Harrison, Electron affinities of the first-row atoms revisited. Systematic basis sets and wave funcions, J. Chem. Phys. 96 (1992) 6796–6806.
[95] J. Tomasi, M. Persico, Molecular interactions in solution: an overview of methods based on continuous distributions of the solvent, Chem. Rev. 94 (1994) 2027–2094.
[96] V. Kumar, M. Chawla, L. Cavallo, A. Basit Wani, A. Manhas, S. Kaur, A. Poater, H. Chadar, N. Upadhyay, Complexation of trichlorosalicylic acids by alkaline and first row transition metals as a switch for their antibacterial activity, Inorg. Chim. Acta 469 (2018) 379–386.
[97] T.K. Das, A. Poater, Review on use of heavy metal deposits from water treatment waste towards catalytic chemical syntheses, Int. J. Mol. Sci. 22 (2021) 13383.
[98] I. Mayer, Charge, bond order and valence in the ab initio SCF theory, Chem. Phys. Lett. 97 (1983) 270–274.
[99] I. Mayer, Bond order and valence: relations to Mulliken's population analysis, Int. J. Quant. Chem. 26 (1984) 151–154.
[100] A. Poater, A. Gallegos Saliner, M. Solà, L. Cavallo, A.P. Worth, Computational methods to predict the reactivity of nanoparticles through structure-property relationships, Expert Opin. Drug Deliv. 7 (2010) 295–305.
[101] A. Poater, S.V.C. Vummaleti, E. Pump, L. Cavallo, Comparing Ru and Fe-catalyzed olefin metathesis, Dalton Trans. 43 (2014) 11216–11220.
[102] A. Casitas, A. Poater, M. Solà, S.S. Stahl, M. Costas, X. Ribas, Molecular mechanism of acid-triggered aryl-halide reductive elimination in well-defined aryl-Cu-III-halide species, Dalton Trans. 39 (2010) 10458–10463.
[103] L. Falivene, R. Credendino, A. Poater, A. Petta, L. Serra, R. Oliva, V. Scarano, L. Cavallo, SambVca 2. A web tool for analyzing catalytic pockets with topographic steric maps, Organometallics 35 (2016) 2286–2293.
[104] A. Poater, L. Cavallo, Comparing families of olefin polymerization precatalysts using the percentage of buried volume, Dalton Trans. (2009) 8878–8883.
[105] A. Poater, B. Cosenza, A. Correa, S. Giudice, F. Ragone, V. Scarano, L. Cavallo, SambVca: a web application for the calculation of buried volumes of N-heterocyclic carbene ligands, Eur. J. Inorg. Chem. (2009) 1759–1766.
[106] L. Falivene, Z. Cao, A. Petta, L. Serra, A. Poater, R. Oliva, V. Scarano, L. Cavallo, Towards the online computer-aided design of catalytic pockets, Nat. Chem. 11 (2019) 872–879.
[107] P. Geerlings, E. Chamorro, P.K. Chattaraj, F. De Proft, J.L. Gázquez, S. Liu, C. Morell, A. Toro-Labbé, A. Vela, P. Ayers, Conceptual density functional theory: status, prospects, issues, Theor. Chem. Acc. 139 (2020) 36.